1 Introduction

The goal of this work is to optimize the design and control of a soft, passive tentacle swimmer to maximize average thrust and velocity. Modeling and understanding the fluid-structure interactions between compliant soft bodies and water is highly complex, resulting in nonlinear behaviors that make these systems difficult to describe analytically. A data-driven approach is therefore required, leveraging a large number of simulations to train surrogate models and optimize the objectives. The simulated data, although not experimentally validated, are expected to capture the correct trends and orders of magnitude, making them suitable for guiding preliminary design decisions. Based on this, the study aims to support the future development of energy-efficient, compliant swimmers for underwater exploration or inspection tasks.

2 Design problem

The passive tentacle is actuated in one degree of freedom, following a pitching motion around the axis normal to the base. As shown in Figure 1, the tentacle geometry is characterized by its length l (between 10 and 60 cm), fixed decreasing diameters ($d_{\text{base}} = 20$ cm, $d_{\text{tip}} = 5$ cm), and a composition ratio c (between 0 and 1), which defines the relative length of two materials with different stiffnesses: Dragon Skin™ (stiffer) and Ecoflex™. The control input is a sawtooth signal with amplitude A (between 5° and 135°) and frequency f (between 0.01 and 3.0 Hz), defined through its truncated Fourier series as:

$$A(t) = A - A \cdot \left(\frac{1}{2} - \frac{1}{\pi} \sum_{k=0}^{3} \frac{(-1)^k \sin\left(2\pi(k+1)ft\right)}{k+1} \right)$$

This asymmetric signal is designed to generate a non-zero average thrust: the tentacle extends slowly and recoils rapidly, resulting in a stronger fluid reaction during the retraction phase.

The design is optimized with respect to two key performance objectives: average thrust and forward velocity. These objectives are partially correlated but not equivalent, and optimizing both enables the identification of trade-offs between force generation and movement speed. It is worth noting that the product of thrust and velocity corresponds to the mechanical propulsion power delivered to the fluid.

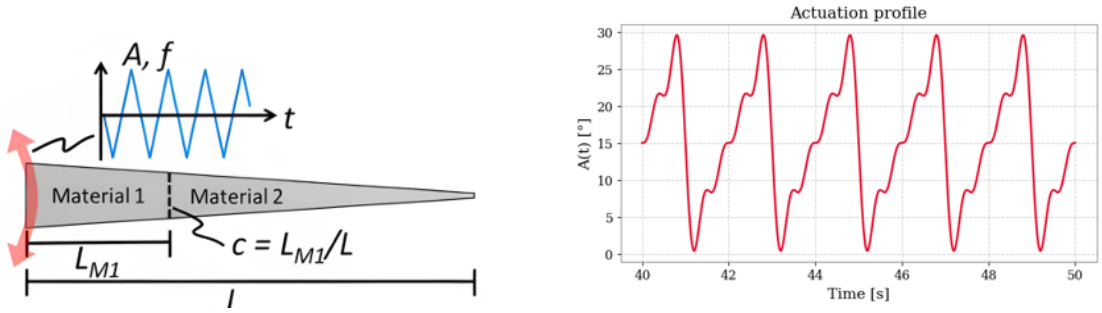

Figure 1: Encoding variables and actuation profile

Since the size of the design space is relatively small (four parameters: l, c, A, and f), and no evident correlation exists between the parameters to be optimized, dimensionality reduction is neither performed nor required. Given the relatively short runtime of each simulation (less than 20 seconds), the initial dataset used to train the surrogate model was generated through a full factorial Design of Experiments, using uniform discretization over the four key parameters. Each parameter was sampled uniformly, and all combinations were simulated, resulting in a dense parameter grid (grid size of 8 per dimension).

3 Data capture

Data were obtained from simulations over one minute of tentacle motion, and the average thrust and velocity were computed. Figure 2 shows the multibody modeling and actuation of the soft structure, together with the simulated behavior for $l = 40$ cm, $c = 0.4$, $f = 0.5$ Hz, and $A = 60°$. The periodic nature of the actuation is clearly visible, along with the initial transient caused by inertial effects, which motivates the use of long simulation times to obtain reliable average values.

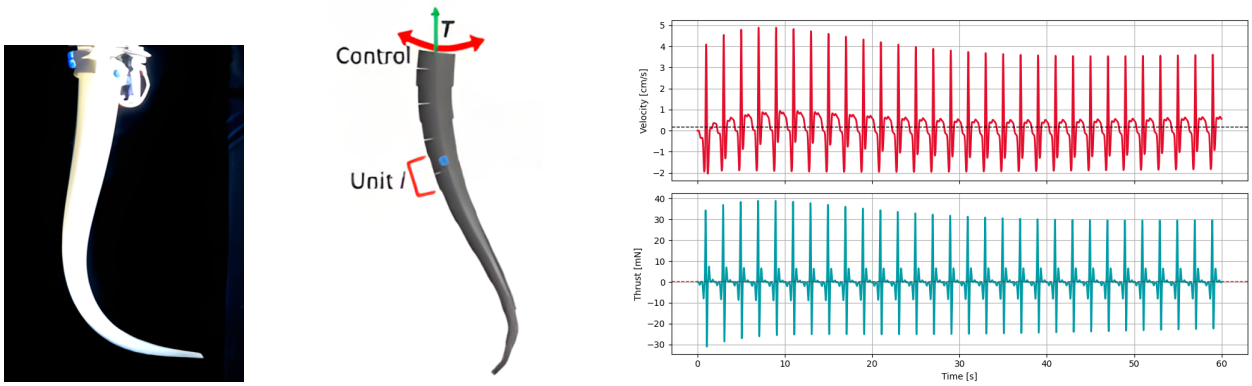

Figure 2: Soft tentacle, multibody simulation and results

Using a lumped-parameter method [1], the tentacle is discretized into a set of frustum-shaped masses, connected to each other by torsional springs and dampers, which allow for bending deformation of the soft body. Each mass has a length of 2.5 cm. The silicone parameters (listed in Table 1) are estimated from commercial data, the drag coefficient is taken from [1], and both the spring coefficient and the moment of inertia are derived from standard beam theory (see Table 2).

Table 1: Material and fluid parameters

Parameter	Value
Silicone density (kg/m^3)	1070
Ecoflex™ E (Pa)	$8.0 \cdot 10^3$
Dragon Skin™ E (Pa)	$4.25 \cdot 10^4$
Ecoflex™ damping factor (N·m·s/rad)	0.05
Dragon Skin™ damping factor (N·m·s/rad)	0.10
C_D	2.0

Table 2: Beam-theory-based quantities

Quantity	Expression
Mass moment of inertia	$I_i = \frac{1}{12} m_i L_i^2$
Geometric moment of inertia	$J_i = \frac{\pi \bar{d}_i^4}{64}$
Spring coefficient	$k_i = \frac{3 E_i J_i}{4 L_i}$

For each element, hydrodynamic, elastic, and damping moments contribute to inertia as follows:

$$\alpha_i = -\frac{M^{\text{stiff}}_{\text{left},i} + M^{\text{stiff}}_{\text{right},i} + M^{\text{damp}}_{\text{left},i} + M^{\text{damp}}_{\text{right},i} + M^{\text{hydro}}_i}{I_i}$$

$$M^{\text{stiff}}_{\text{left},i} = k_i(\theta_i - \theta_{i-1}), \quad M^{\text{stiff}}_{\text{right},i} = k_{i+1}(\theta_i - \theta_{i+1})$$

$$M^{\text{damp}}_{\text{left},i} = b_i(\omega_i - \omega_{i-1}), \quad M^{\text{damp}}_{\text{right},i} = b_{i+1}(\omega_i - \omega_{i+1})$$

$$M^{\text{hydro}}_i = \frac{1}{12}\rho_w C_D A_{\text{lat},i} L_i^2 \cdot \frac{U^{\perp}_{i+1} - U^{\perp}_i}{L_i} \cdot \frac{U^{\perp}_{i+1} + U^{\perp}_i}{2}$$

For each time step, thrust and velocity are then computed as:

$$\begin{cases} T(t) = F_{\text{drag}}(t) + F_{\text{added mass}}(t) \\ v(t) = \displaystyle\int_0^t \frac{T(\tau) - F_{\text{resist}}(v(\tau))}{m}\, d\tau \end{cases}$$

A stiff implicit integrator (BDF method from `solve_ivp`) is used with high temporal resolution (60,000 points) and strict tolerances (`atol` $= 10^{-6}$, `rtol` $= 10^{-4}$). The simulation data are noise-free and fully deterministic; while this ensures consistency across runs, it does not account for real-world variability.

The use of high temporal resolution (60,000 steps per minute) ensures accuracy but comes at the cost of increased simulation time. As anticipated in Section 1, these results have not been experimentally validated; although they reflect realistic behavior, they should be interpreted as idealized predictions of the system's performance.

4 Data-driven method

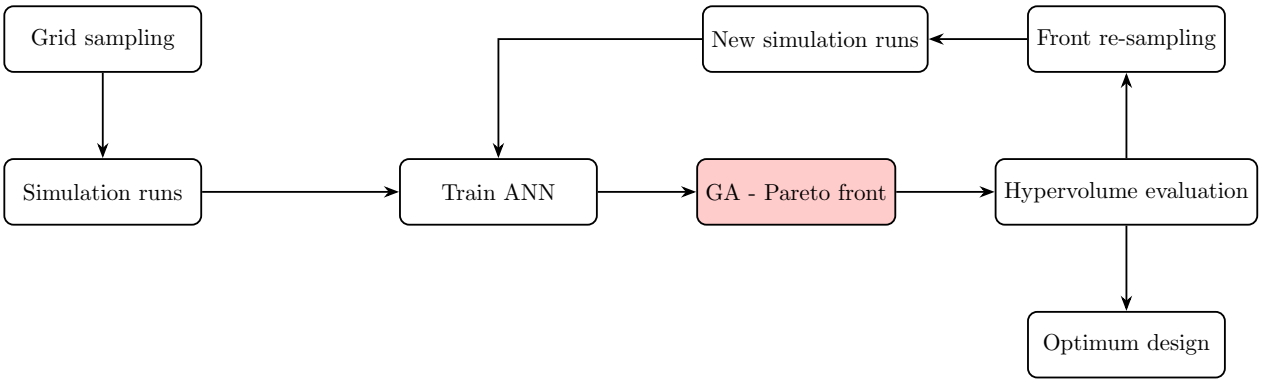

Figure 3: Data-driven optimization

The adopted data-driven optimization pipeline is shown in Figure 3. Initial data are collected through full factorial DoE and used to train an artificial neural network surrogate model. The architecture is a multi-layer perceptron with two hidden layers, which regresses thrust and velocity as functions of the design space parameters. It is trained using `MSE` loss, `Adam` optimizer with learning rate $\eta = 10^{-3}$, and early stopping with a 90–10% split.

A multi-objective Genetic Algorithm is chosen to optimize two conflicting objectives in a framework where no analytical expression of the objective function is available, as the design space is explored through a population of individuals. A population size of 200 ensures sufficient coverage without excessive computational cost; the crossover probability is set to 0.9 to maintain high evolutionary pressure and approximate the Pareto front from early generations; the mutation rate is 1/4, so that, on average, one variable is mutated per individual per generation. The algorithm minimizes the vector `[-thrust, -velocity]` to compute the Pareto front.

Once the optimization for a given dataset is completed, *active learning* is implemented: Pareto points are perturbed with Gaussian noise, and simulations are performed for all of them to enrich the dataset with informative samples, in order to better exploit the most promising regions of the design space. Once the new dataset is collected (adding 50 new samples at each iteration), the surrogate model is retrained and the optimization is repeated. Variable perturbations are assumed to be independent, with standard deviations for l, c, f, and A equal to 0.2 m, 0.2, 0.4, and 10°, respectively.

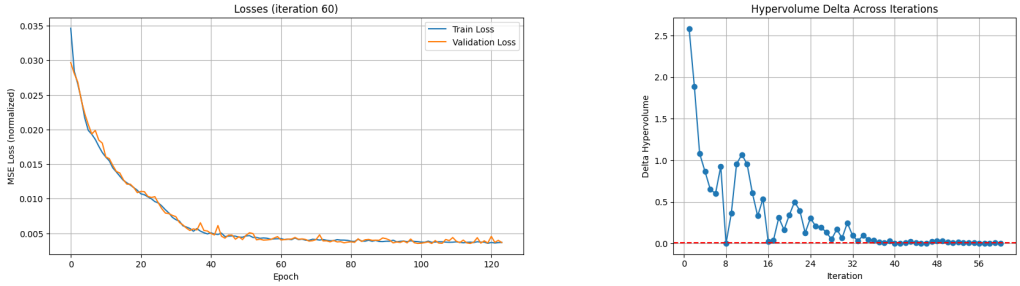

Figure 4: Surrogate model training and Δ_{HV} over iterations

The stopping criterion is based on hypervolume evaluation. Hypervolumes measure the portion of the objective space (`[-thrust, -velocity]`) dominated by the Pareto front with respect to a fixed reference

point, here set to `[0, 0]`. Active learning stops when this metric reaches a *plateau*, that is, when the optimization process no longer yields a diverse distribution. In practice, this occurs when Δ_{HV} (the absolute difference between successive hypervolumes) remains below 0.01 mW for 5 consecutive iterations. Figure 4 shows the training and validation losses, along with the evolution of Δ_{HV} over iterations, which naturally decreases in a non-monotonic way due to the stochastic nature of the process, up to the 60^{th} iteration.

5 Results

Table 3: Best results by objective

Objective	l [m]	c [-]	f [Hz]	A [°]
Thrust	0.317	0.645	3.000	135.0
Velocity	0.171	0.815	1.435	67.5

Table 4: Pareto front summary statistics

Metric	Min	Max	Mean
Thrust [mN]	7.33	53.36	25.57
Velocity [cm/s]	5.29	7.67	6.35

Results from the multi-objective Genetic Algorithm optimization are reported in Table 3.

Maximum thrust is achieved for $l = 31.7$ cm, where the tentacle effectively balances two contributions: high peripheral velocity, favorable for propulsion, and structural compliance due to flexural deformability, which limits the efficient transmission of force to the surrounding fluid. On the other hand, velocity is maximized at $l = 17.1$ cm, as the shorter tentacle has lower mass and reduced surface area, resulting in lower drag resistance. Additionally, the increased stiffness associated with shorter lengths minimizes deformation and enables a more efficient conversion of motion into forward movement.

An optimal material ratio of $c = 0.645$ for thrust suggests that a certain level of compliance is necessary to generate higher forces, as it enables greater bending, especially in the faster part of the sawtooth wave. However, when stiffness is too low (small c), excessive deformation causes energy losses, reducing thrust (see Figure 6 for further details). Conversely, high stiffness ($c = 0.815$) is advantageous for velocity: a less compliant tentacle transmits passive motion more effectively from base to tip and minimizes viscous resistance by maintaining more favorable shapes during motion. The preference for relatively high stiffness values can be explained by the steepness of the actuation signal; a smoother waveform might instead benefit from a softer structure.

Thrust is maximized at the highest tested frequency, $f = 3$ Hz. This is because each oscillation cycle generates an impulse, and increasing the number of cycles per unit time leads to a higher average impulse, and thus greater thrust. At this frequency, the optimal tentacle design can still follow the actuation effectively. Since $f = 3$ Hz represents the upper limit of the tested range, it is reasonable to expect that thrust would continue to increase with frequency, up to the point where the tentacle can no longer follow the motion due to its compliance. In such cases, shorter tentacles would likely be required to maintain performance. On the other hand, the optimal frequency for velocity is $f = 1.435$ Hz. Frequencies that are too high lead to excessive oscillations and drag, resulting in incoherent motion where the tentacle tip lags behind, reducing net forward velocity. Conversely, frequencies that are too low result in slow and suboptimal movement.

Finally, the highest oscillation amplitudes A lead to greater thrust, as they displace more fluid and enhance the reactive force during the closing phase of the sawtooth wave, particularly due to its steeper slope. In contrast, a lower amplitude ($A = 67.5°$) is optimal for maximizing velocity, as it reduces fluid resistance while still generating sufficient thrust for effective propulsion. It is important to note that the motor is assumed to be ideal, capable of reproducing all input motions without limitations; introducing actuation constraints would likely alter the results.

Table 4 shows the range of values along the Pareto front depicted in Figure 4. Notably, thrust and velocity span wide intervals, as optimizing one often leads to suboptimal values of the other. This observation is consistent with typical swimming strategies: swimmers must not only generate strong propulsion, but also adapt their body and movement to the surrounding fluid to minimize resistance and increase speed. Similarly, since the actuation is entirely passive, both design and motion must be adapted to reflect the complex interactions with water.

Obayashi et al. [1] report an optimal velocity and thrust of 6.2 cm/s and approximately 38 mN for a different tentacle-based robot, 20 cm in length, with a distinct actuation configuration. Although the setup differs, most notably in the motion profile and number of tentacles, the reported velocity and thrust are of the same order of magnitude as the values in Table 4. Differences can be attributed to the system architecture and, in particular, to the actuation strategy, which induces alternative dynamic behavior in the actuated tentacle. Yet, these benchmark results, which have been validated experimentally, demonstrate the effectiveness of the proposed method.

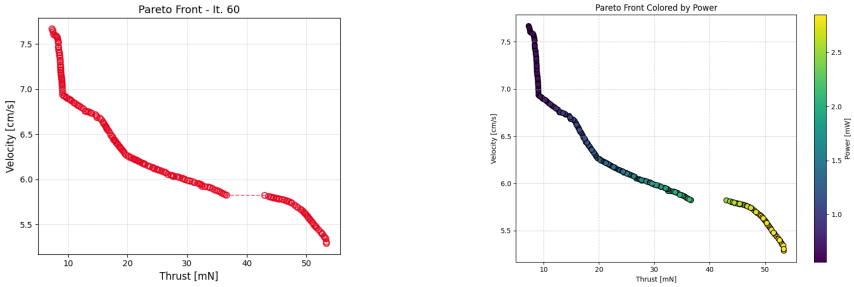

Figure 5: Final Pareto front, colored by generated power

Figure 5 shows the final Pareto front (60^{th} iteration) and its relation to the generated power, which is naturally higher where the product of the two objective functions is greater. Figure 6 illustrates the effects of all parameters on thrust and velocity across the Pareto front. Various values of c appear along the front for both thrust and velocity, although clear benefits are observed near the respective optima. Thrust increases almost linearly with frequency, while velocity reaches a maximum at the optimal f and then decreases due to increased drag and oscillations. Thrust benefits considerably from higher amplitudes, while velocity is maximized at intermediate values but remains relatively high even at the upper limit, indicating that greater thrust contributes significantly to forward motion. Finally, regarding length l, Pareto-optimal solutions are concentrated in two narrow regions: one at shorter lengths, which favors velocity by minimizing mass and drag, and one at longer lengths, which enhances thrust through greater fluid interaction. Thus, even small deviations from these configurations lead to a significant drop in overall performance.

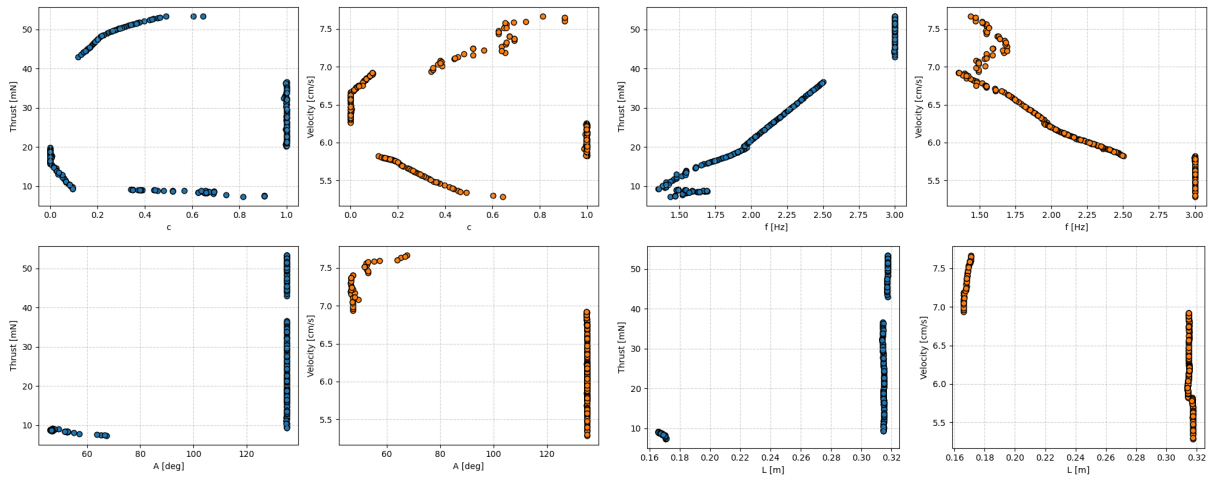

Figure 6: Effects of design parameters on thrust and velocity (Pareto front)

Figure 7 shows the effect of each parameter on thrust (top) and velocity (bottom), as predicted by the surrogate model. In each case, three parameters are fixed to their respective optimal values, and the remaining one is varied. Regarding l, a single clear maximum is observed for thrust, while velocity exhibits several local maxima, one of which coincides with the optimal length for thrust, as previously

noted. The material ratio c shows limited influence on thrust but has a more pronounced effect on velocity. Frequency f has a strong impact on thrust and presents a clear local optimum for velocity. The same applies to amplitude A, where fluid-structure interactions induce trade-offs that affect both objectives.

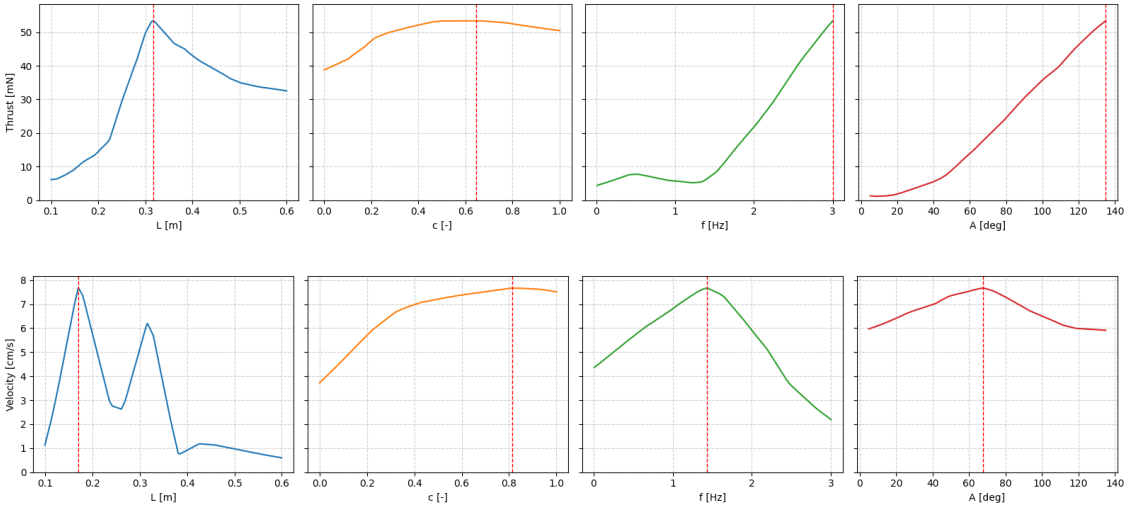

Figure 7: Optimal thrust and velocity vs. L, c, f, and A

6 Discussion and conclusion

The proposed data-driven optimization framework proved effective in identifying passive tentacle configurations that achieve high average thrust and velocity in simulation. The optimal solutions obtained through the Genetic Algorithm, supported by the surrogate model, cover a broad range of performance levels and align well with values reported in the literature for similar systems. This is relevant to soft robot design, where higher velocities enable faster swimming, while greater thrust can compensate for added mass, increased drag, or more demanding tasks, including the presence of external payloads or attachments.

The multi-objective algorithm produced a clear Pareto front, confirming that maximizing one objective may penalize the other due to the inherent compliance of the robot. The proposed method enables the identification of optimal trade-offs. Thrust is favored by softer compositions and large oscillation amplitudes, whereas velocity is maximized with slightly stiffer structures and moderate movements. Tentacle length should be higher for maximizing thrust, while shorter lengths are preferable for optimizing velocity. High frequencies yield greater thrust, but an intermediate range is more suitable for velocity, as it balances impulse generation with reduced drag and oscillatory losses.

The method could be further improved. Results are currently based solely on computer simulations, without empirical validation. Conducting experimental tests on real prototypes would help bridge the *sim2real* gap, as modeling soft robots is inherently complex and subject to non-idealities. Moreover, the control strategy relies exclusively on a sawtooth signal, truncated at the fourth term of its Fourier series, although alternative waveforms or steeper actuation profiles could be encoded as design variables and may significantly affect performance. Finally, an ideal motor has been considered, but the design criteria did not account for efficiency or energy dissipation parameters, even though these are crucial aspects in the development of feasible underwater robots.

References

[1] Nana Obayashi, Carlo Bosio, and Josie Hughes. “Soft passive swimmer optimization: from simulation to reality using data-driven transformation”. In: *IEEE 5th International Conference on Soft Robotics (RoboSoft)* (2022).